JOURNAL OF GEOPHYSICAL RESEARCH, VOL. 98, NO. E9, PAGES 17,099–17,113, SEPTEMBER 25, 1993

Radar Polarization Properties of Volcanic and Playa Surfaces: Applications to Terrestrial Remote Sensing and Venus Data Interpretation

BRUCE A. CAMPBELL

Center for Earth and Planetary Studies, National Air and Space Museum, Washington, D.C.

RAYMOND E. ARVIDSON AND MICHAEL K. SHEPARD

Department of Earth and Planetary Sciences, Washington University, St. Louis, Missouri

The radar polarization properties of lava flows in Hawaii (Kilauea) and Arizona (SP flow), and two playa surfaces (Lunar Lake, Nevada and Lavic Lake, California), are compared to the predicted behaviors of theoretical scattering models. At 5.7 cm and 24 cm wavelengths, Kilauea lava flows can be modeled by a combination of facet and diffuse (dipole-like) scattering. Scattering by rock faces on the scale of the radar wavelength is proposed to account for much of the facet return. The radar echoes at 24-cm wavelength from SP flow are, on average, consistent with entirely diffuse scattering, but there are regions within the flow where circular polarization ratios exceed unity, suggesting a coherent scattering effect. 68 cm data for the lava flows show evidence of radar penetration and volume scattering. The playa surfaces are characterized by polarization properties which in some cases are qualitatively consistent with the first-order small-perturbation model, but the echoes do not closely match the predictions of this model for any reasonable dielectric constant value. These results show that it may be difficult to construct invertible models for the polarization behavior of some surfaces (the playas), whereas for others (the Kilauea lava flows) the scattering properties can be successfully modeled. The first-order small-perturbation model is not appropriate for inverse modeling of most terrestrial lava flows, though very smooth surfaces on Venus may be amenable to the use of this model. High circular polarization ratios observed for SP flow, tentatively attributed here to coherent backscatter, may be analogous to Arecibo observations of high-reflectivity areas on Venus.

Introduction

Imaging radar systems are an important geologic remote sensing tool for terrestrial and planetary applications. The sensitivity of radar backscatter measurements to roughness on cm to meter scales and to variations in bulk dielectric properties makes them useful for mapping out differences in surface morphology, density, and reflectivity. Airborne and spaceborne radar systems are in use and being developed which offer the possibility of rapid high-resolution mapping of terrestrial volcanic surface structure [*Evans et al.*, 1993]. For Venus, microwave remote sensing provides our only view of the surface on a global scale, so interpreting radar data is a crucial part of assembling a geologic framework for this planet [*Saunders et al.*, 1992].

A fundamental issue in radar remote sensing is the relationship between surface roughness and dielectric parameters and the intensity, polarization, and angular dependence of the backscattered wave. Over the past thirty years, several models for surface scattering have been widely used: the quasi-specular or physical optics model [*Hagfors*, 1964; *Pettengill et al.*, 1988; *Tyler et al.*, 1992], the small-perturbation approach [*Barrick and Peake*, 1967], coherent backscatter theory [*Hapke*, 1990], and "diffuse" scattering models [*Ford and Senske*, 1990]. Aspects of these models were often discussed in analyses of terrestrial and planetary radar data [cf., *Schaber et al.*, 1980; *Theilig et al.*, 1989; *Blom et al.*, 1987; *Gaddis et al.*, 1989], but it was difficult to judge their applicability to a particular surface.

Paper number 93JE01541.
0148-0227/93/93JE-01541$05.00

In the last seven years it has become possible to acquire fully polarimetric data (wherein the radar scattering matrix for each resolution cell is measured) with the NASA/Jet Propulsion Laboratory airborne synthetic aperture radar (AIRSAR) system, and these data have opened up many opportunities for surface characterization in terms of radar polarization properties and wavelength/incidence-angle dependence [*Evans et al.*, 1986]. Several authors have considered the issue of surface scattering using these new data, and have compiled backscatter cross-section values for volcanic and playa surfaces [*Plaut*, 1991; *Gaddis*, 1992; *Campbell and Campbell*, 1992; *Arvidson et al.*, 1993]. *Gaddis* [1992] analyzed AIRSAR data for Pisgah volcanic field, and discussed the optimum radar parameters for discrimination of pahoehoe, a'a, and playa surfaces. The shape of the radar backscatter curves and measurements of surface roughness showed that the first-order small-perturbation model was not applicable to many of the lava flows within this region, but the specific nature of scattering from these terrains was not pursued further.

There have also been several recent efforts at creating inverse models for radar scattering. *Van Zyl* [1989] proposed a classification scheme for image pixels based on criteria related to the radar polarization and phase. *Campbell et al.* [1989] modeled the radar return from lava flows as the incoherent sum of four discrete scattering mechanisms (quasi-specular, small-perturbation, dihedral, and unpolarized). While the results of this model for lava flows in Craters of the Moon, Idaho, correlated qualitatively with field-measured roughness, no effort was made to explain the actual nature of scatterers on the surface. *Van Zyl et al.* [1991] estimated the roughness of Pisgah playa and lava flows by inversion of the first-order small-perturbation model, and found a good correlation between radar-derived and measured (from stereo imagery)

topographic parameters. Their results conflict with the conclusions of *Gaddis* [1992] which indicated that the first-order model was not valid for many of the Pisgah surfaces. The applicability of various radar scattering models to specific terrain types is thus still a matter of debate.

Analyses of high-resolution Magellan and Arecibo data for Venus have raised a number of questions regarding backscatter mechanisms. The most controversial of these issues is the nature of the low-emissivity (high reflectivity) surfaces on portions of the planet above ~6053 km radius [*Pettengill et al.*, 1992]. These surfaces exhibit highly variable circular polarization ratios, which in some cases exceed unity [*D.B. Campbell*, pers. comm., 1993]. Preliminary studies of Magellan dual-polarization (HH and VV) data by *Plaut* [1993] show that these low-emissivity regions also have enhanced VV returns in some locales.

In this paper, we address the polarization properties of terrestrial volcanic and playa terrains as a test of current models for radar scattering and to aid in the interpretation of data for Venus from Magellan and Arecibo. These terrain types were chosen because they represent a wide range of roughness, from extremely rough blocky and a'a lava flows to the very smooth playa surfaces. Much of the surface of Venus is dominated by volcanic terrain [*Head et al.*, 1992], so terrestrial lava flows are a good starting point in the search for surfaces analogous to those seen by Magellan. Comparison of Magellan and terrestrial airborne radar data has shown, however, that some Venusian lava flows and dark crater ejecta deposits have very low radar returns, comparable to those of terrestrial playas [*Arvidson et al.*, 1992], so two of these lacustrine surfaces have been included in this study. We will first examine the polarization properties of some widely used models for the radar scattering process. We will then present the results of our radar analyses of the volcanic and playa surfaces, and discuss the impact of these data on three remote sensing issues: (1) what scattering models are most applicable to the different terrain types, (2) how much surface structural and dielectric information can be extracted from polarimetric data, and (3) what can we learn from the combination of Magellan and Arecibo radar measurements for Venus?

Scattering Models

The backscatter from a surface will be described here in terms of the specific cross section σ_0 for a chosen combination of transmit and receive polarizations. These combinations are denoted by pairs of letters, where the first refers to the transmitted polarization, and the second to the received polarization. H refers to horizontal linear, V to vertical linear, R to right-circular, and L to left-circular polarization. The radar wavelength is denoted by λ and the incidence angle by ϕ. For reference, Magellan acquires data in HH and VV polarizations, while Arecibo uses predominantly LL and LR (dual circular) polarizations. Both systems operate at 12.6 cm wavelength. The AIRSAR system collects the full scattering matrix for each pixel at *C* (5.7 cm), *L* (24 cm), and *P* (68 cm) band wavelengths.

The Quasi-Specular Model and "Small-Facet" Scattering

One of the earliest scattering models to gain wide acceptance was developed in connection with radar studies of the Moon in the 1960's. It was noted that polarized (opposite-sense) circular echoes exhibited a rapid drop in power within 5-15° of the nadir, and a slower decline at more oblique angles. The depolarized (same-sense) circular echoes declined proportional to $\cos^n\phi$, where n varied from 1.5-1.75 [*Hagfors*, 1967]. These observations led to the definition of two scattering components: the "quasi-specular" return, comprised of reflections from relatively smooth surface regions tilted to face the incoming radar beam, and "diffuse" echoes, eventually attributed to scattering by randomly oriented cracks and edges [*Hagfors and Evans*, 1968].

Hagfors [1964] modeled the quasi-specular component as the echoes from a surface whose radius of curvature is everywhere large with respect to the radar wavelength. This permits the surface roughness to be characterized by a statistical distribution of slopes; only those surface regions perpendicular to the incident beam will return a specular echo. Under these constraints, the angular backscatter behavior of a surface is dependent only upon the rms slope (the ratio of the height standard deviation to the surface height correlation length). Large "hills" far apart will scatter as effectively as small hills close together, within the limits that the radius of curvature must be large with respect to the wavelength.

The predictions of the Hagfors model in terms of polarization and angular dependence are noted below. These results are based on a surface with a Gaussian surface height distribution and an exponential height autocorrelation function. Note that the backscattered power scales linearly with the Fresnel reflectivity, as expected for returns from mirror-like facets. Likewise, this model predicts no depolarization of plane-polarized waves, and the sense of circular polarization is reversed upon reflection.

$$\mathrm{HH} = \mathrm{VV} = \mathrm{LR} = \frac{\rho C}{2}\left[\cos^4\phi + C\sin^2\phi\right]^{-1.5} \quad (1)$$

$$\mathrm{HV} = \mathrm{LL} = 0 \quad (2)$$

where ρ is the Fresnel reflectivity evaluated at normal incidence and C is the inverse mean square slope [*Hagfors*, 1964].

This model is often used for characterizing the large-scale roughness of planetary surfaces [*Pettengill et al.*, 1988; *Ford and Pettengill*, 1992], but recent analysis of Magellan data by *Tyler et al.* [1992] has shown that other surface slope distributions provide a better match to returns for some echoes, particularly from rougher areas. In this paper, we are less concerned with the angular scattering behavior of facet returns (which is determined by the statistical distribution of surface slopes) than with polarization properties, which do not change from one statistical surface model to another.

Another mechanism that must be considered is "small facet" scattering. While the Hagfors model deals with echoes from plane facets, these scatterers are assumed to be large with respect to the radar wavelength. As surface roughness increases, the size of the largest effective facets on the surface will decrease, and the returns will no longer have the strong coherent echo peak seen at nadir for the quasi-specular model. Once the Hagfors model assumptions break down, however, we do not immediately transition to a diffuse (or dipole-like) scattering regime. There will still be enhancement of the like-polarized (HH and VV) components over the cross-polarized echoes (HV and VH) as long as the scattering objects are a significant fraction of the radar wavelength in extent. A small rock on the surface will have poorly directed (scattered over a large range of angles) reflections from its faces, and its edges will scatter as dipole elements.

Diffuse Model

Some surfaces may be modeled as a collection of randomly oriented small dipole elements. Such a field of elements will the have the following polarization properties [*Mack and Reiffen*, 1964]:

$$\sigma_o = A \cos^n\phi \tag{3}$$

$$HH = VV = 3\,HV \tag{4}$$

$$LL = LR = 2\,HV \tag{5}$$

Where A is a scaling factor proportional to the total number of such elements within each resolution cell. The exponent n on the cosine term in this expression will vary with the spatial distribution of the dipoles: there will be a simple cosine dependence (n=1) if the dipoles are randomly distributed in space, while a field of flat-lying dipoles will have n=2. Radar echoes from the Moon at large incidence angles were found to match this model, with n=1.5-1.75 [*Hagfors and Evans*, 1968].

Campbell et al. [1989] used a "diffuse" scattering component in their inverse model which was assumed to have equal power in all echo polarizations. An echo with no polarization dependence would likely be generated only by multiple scattering of the radar energy, which produces a weak return unless the surface reflectivity is very high. The diffuse model used here is thus more physically realizable.

The Small-Perturbation Model

One important scattering model deals specifically with roughness whose mean height is a small fraction (<5%) of the radar wavelength. An excellent review of this model is contained in *Barrick and Peake* [1967], and the practical limitations on various implementations of the model are well covered in *Ulaby et al.* [1987]. Since the model solution is based upon slight perturbations from a flat surface, rms heights on the scale of the radar wavelength are prohibited; this constraint also prevents a geometric optics approach to this scattering problem, which is possible for the large-scale roughness of the Hagfors/Kirchhoff models. This model was used by *D.B. Campbell et al.* [1992] to characterize the roughness of Venus crater ejecta deposits.

To first order, the small perturbation specific backscatter cross-section is [*Barrick and Peake*, 1967; *Ulaby et al.*, 1987]:

$$\sigma_o = 8\,k^4 h^2 \cos^4\phi\,|\alpha_{ij}|^2\,W(2k\sin\phi) \tag{6}$$

$$\alpha_{hh} = \frac{\varepsilon - 1}{\left[\cos\phi + \sqrt{\varepsilon - \sin^2\phi}\right]^{0.5}} \tag{7}$$

$$\alpha_{vv} = \frac{(\varepsilon - 1)\left[(\varepsilon - 1)\sin^2\phi + \varepsilon\right]}{\left[\varepsilon\cos\phi + \sqrt{\varepsilon - \sin^2\phi}\right]^{0.5}} \tag{8}$$

$$\alpha_{ll} = \frac{(\alpha_{hh} - \alpha_{vv})}{2} \tag{9}$$

$$\alpha_{lr} = \frac{(\alpha_{hh} + \alpha_{vv})}{2} \tag{10}$$

$$\alpha_{hv} = 0 \tag{11}$$

where k is the radar wavenumber, h is the surface height standard deviation, ε is the surface dielectric constant, and W is the normalized surface roughness spectrum. It can be seen that σ_0 is proportional to the power in the surface roughness spectrum at a spatial wavelength of $\lambda/2$ projected onto the ground. In the first order approximation, the polarization ratios (HH/VV, LL/LR) are independent of the specific surface roughness terms, and depend only upon the dielectric constant and the radar incidence angle. Figure 1 shows the HH/VV and LL/LR ratios for the first-order small-perturbation model, with dielectric constant values from 2 to 7. As shown above, the ratio of the circular components is dependent upon the ratio of the HH and VV returns. It is also important to note that the first-order model always predicts HH/VV ratios less than or equal to unity.

The first-order small-perturbation model is most commonly used, but it is possible to carry the expansion to higher orders [*Ulaby et al.*, 1987; *Barrick and Peake*, 1967]. At second order, the model predicts an HV backscatter component, and can be used over a somewhat larger range of surface roughnesses. The second-order model is much more complicated than that shown

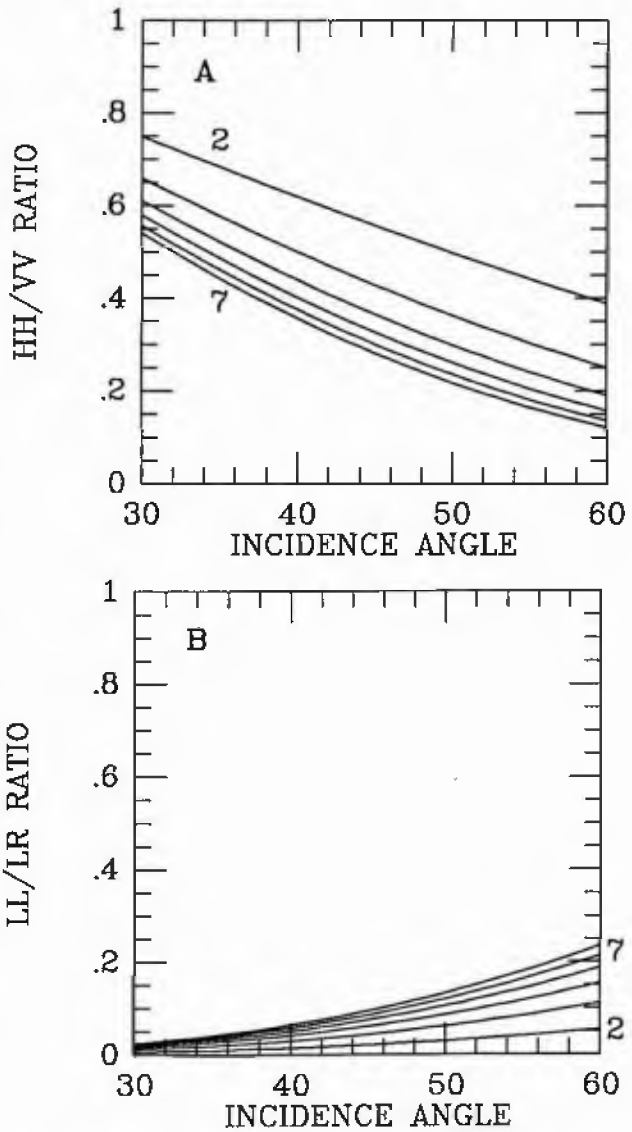

Fig. 1. (a) Linear (HH/VV) and (b) circular (LL/LR) polarization ratios predicted by the first-order small-perturbation model. See text for description of model. Results shown for dielectric constant values of 2, 3, 4, 5, 6 and 7.

above, and the ratios between polarizations are functions of the dielectric constant, rms height, and correlation length. These difficulties underscore a primary dilemma in radar backscatter: for roughness on the scale of the radar wavelength, a mathematical analysis of the scattering process may become exceedingly complex. Recent efforts in theoretical scattering analysis [*Fung et al.*, 1992] show promise for resolving some of these problems. In this work, we focus on the first-order model to determine its range of applicability.

Dihedral Scatterers and Coherent Backscatter

A type of scattering element which could become important on blocky lava flows or in regions of high Fresnel reflectivity is the dihedral joint. Returns from a suite of such elements would exhibit enhanced HH echoes (HH/VV>1.0) and strong LL returns (since there are two reflections to reverse the sense of circular polarization of the wave). The primary concern with this model is the fact that the wave undergoes two reflections, which greatly reduces the backscatter cross section. Roughness at the sub-wavelength scale on either face of the joint will further degrade the return. The polarization properties of a dihedral joint with its lower face horizontal are (for scattering in the plane of incidence):

$$\frac{VV}{HH} = t = \frac{\cos^2(\phi + \phi_1)\sin^2(\phi - \phi_2)}{\cos^2(\phi - \phi_1)\sin^2(\phi + \phi_2)} \tag{12}$$

$$\phi_1 = \sin^{-1}\left(\frac{\sin\phi}{\sqrt{\varepsilon}}\right) \tag{13}$$

$$\phi_2 = \sin^{-1}\left(\frac{\cos\phi}{\sqrt{\varepsilon}}\right) \tag{14}$$

$$\frac{LL}{LR} = (1 + \sqrt{t})/(1 - \sqrt{t}) \tag{15}$$

Note that LR will go to zero for a perfectly conducting surface (t=1.0), and the LL/LR ratio is always greater than unity. This type of echo is not likely to be important unless the surface is comprised of smooth-sided rocky "cubes" or has high Fresnel reflectivity.

A second mechanism which could (perhaps more easily) produce high LL/LR ratios is the "coherent backscatter" model [*Hapke*, 1990], proposed to explain the very large radar albedo and high (>1.0) LL/LR ratios for the icy Galilean satellites [*Ostro et al.*, 1992]. In this model, the radar backscatter arises from instances of two or more reflections off discrete scatterers in a relatively transparent matrix. Any single path taken by the radar as it hits these objects and returns to the observer is mirrored by a ray traveling in the opposite direction. The result is a two-fold enhancement in like-polarized (LL, HH, and VV) energy due to the coherent addition of these paired rays. The LR returns do not benefit from this effect, so such a surface could produce LL/LR ratios up to 2. *Hapke* [1990] discussed this model in the context of reflective scatterers embedded in ice, but it could equally well apply to rock surfaces in air. The magnitude of such a multiple-scattered return may be extremely small if the individual scatterers distribute the incident power over a wide range of angles or if the intrinsic reflectivity of the material is low.

Ground Penetration and Volume Scattering

If a surface has a low imaginary dielectric constant ("low loss" material), then a significant fraction of the incident energy may propagate into the target material. The propagation depth of the energy depends upon the radar wavelength and the microwave loss properties of the medium. In porous materials or at large radar wavelengths, volume scattering can be an important component of the backscatter. The presence of water in a soil, even at a few weight percent, will rapidly reduce the depth of penetration. If the radar energy does penetrate into the material, it may be scattered by dielectric discontinuities such as voids, inclusions, or interfaces. These echoes may be weaker than those of surface scatterers due to losses upon transmission and propagation, but if the surface roughness is slight they may still play a major role in the observed return.

The polarization and angular backscatter properties of such returns will depend upon the sub-surface scattering mechanism and the dielectric contrasts along the propagation path of the radar energy. A simple approach which demonstrates the effect of a surface interface is to treat the buried scatterers as randomly oriented dipoles, and the surrounding matrix as a layer with a single dielectric constant. If the dielectric constant is ε, then the volume-scattered energy will have the following polarization properties due to transmission effects [*Stratton*, 1947]:

$$\frac{HH}{VV} = \cos^4[\phi - \sin^{-1}(\frac{\sin\phi}{\sqrt{\varepsilon}})] \tag{16}$$

$$\frac{HV}{VV} = \frac{1}{3}\cos^2[\phi - \sin^{-1}(\frac{\sin\phi}{\sqrt{\varepsilon}})] \tag{17}$$

$$\frac{LL}{LR} = 1.0 \tag{18}$$

Burying the dipoles in a matrix has the effect of lowering the HH/VV ratio (which is 1.0 for surface dipoles) and the HV/VV ratio (which is 1/3 for surface scatterers). The LL/LR and HV/LL ratios are unchanged by the presence of the dielectric interface, since the dipole echoes have random phase between H and V components. If the buried scatterers were facets, then the LL/LR ratio would be quite different because the H and V returns would have some degree of coherence. These polarization properties are only guides for interpretation; the subsurface scatterers may vary in size, shape, and dielectric contrast, and the surrounding medium may change in permittivity laterally or with depth.

Radar Observations Of Lava Flow Surfaces

Kilauea Lava Flow Units

The Kilauea lava sample areas represent a typical spectrum of basaltic flow types, from smooth ponded flows with less than 2 cm rms height, up to rubbled, spiny a'a flows with 50-100 cm of relief. Data for all study areas were collected by the NASA/JPL AIRSAR system. Each scene has been corrected for phase and crosstalk errors [*van Zyl*, 1990], using in-scene corner reflectors wherever possible (the SP scenes lacked these reflectors, so phase and cross-talk corrections were made using the image data). The absolute accuracy of the calibrated backscatter cross-sections may vary from 1-3 dB depending on the surfaces measured, but the consistency of the data from one part of a scene to another is very good [*van Zyl*, 1990; *Freeman et al.*, 1992]. The systematic errors in the polarization ratio values (HH/VV, LL/LR) are more difficult to quantify, but should be relatively small for scenes calibrated with the corner reflectors. The dominant source of error in the ratio values is likely to be insufficient averaging of pixels, so we have chosen large sample areas for each site.

Fig. 2. *L* band (24 cm) HV-polarization radar image of Kilauea Volcano, Hawaii, showing locations of 10 surface sample regions. Location numbers keyed to descriptions in Table 1. Radar flightline at top of image; caldera center approximately 155° 16' W, 19° 25' N. Image width 18 km; data geometrically rectified to 10 m pixel spacing.

We selected 10 surface units to study, shown in Figure 2. These units are identical to those presented by *Campbell and Campbell* [1992] as a comparison to Magellan data for Venus, and the incidence angles and backscatter cross-sections for each site are tabulated in that paper. The range of incidence angles for the Kilauea data is 27°-61°, with each unit subtending some portion of this range. Table 1 describes the general roughness properties of each surface. Each site was defined by one or more rectangular boxes, and the backscatter power values for HH, VV, LL, LR, and HV polarizations were averaged in 1° incidence angle bins.

As part of a study of volcanic microtopography, we measured surface height profiles for three sites along the 1982 lava flow using a laser ranging device [*Campbell and Garvin*, 1993]. The surface height was measured every 5 cm over profile lengths of 5-8 m, and the rms heights for each site were calculated after profile detrending (Table 1). Even the very smooth ponded pahoehoe surface had an rms height of 1.4-1.1 cm (the range represents values for the raw profile data and after a 1-m high-pass filter), due to a ubiquitous covering of broken glass chips. Also included in Table 1 are values of rms height measured by *Gaddis et al.* [1989, 1990] for the December 1974 lava flow. Their data indicate a range of rms heights of 1.9-5.2 cm for the portion of the flow we used as a pahoehoe sample area in the AIRSAR scene, and values up to 24.4 cm for the a'a portions of the flow. These data were collected over 7-9 m profiles at 2.54 cm intervals, and no high-pass filtering was performed prior to calculating a standard deviation. As such, these data are best taken as upper bounds on the rms height for horizontal scales of a meter or less, since roughness at larger scales can strongly influence the calculated value if no filtering is carried out.

The dielectric properties of the Kilauea lava flows have not been measured, but the large range of vesicularity among the various surfaces implies at least some variability in this parameter. The younger pahoehoe units tend to have well-

TABLE 1. SAR Target Site Roughness Data

	Site Name	Surface Description	RMS Height (cm)
Kilauea Volcano, Hawaii			
1	Mauna Iki a'a	platy a'a	
2	Mauna Iki 1919-1920 pahoehoe	billowy pahoehoe with many collapses	
3	Mauna Iki 1919-1920 a'a	jumbled plates and rubble	
4	December 1974 a'a	very rough spiny, plate, or ball a'a	10.4-24.4
5	December 1974 pahoehoe	sheet pahoehoe with ropy patches	1.9-5.2
6	1982 a'a	moderately rough platy a'a	8.3-9.6
7	1982 pahoehoe	ropy channelized pahoehoe	4.0-6.9
8	1982 ponded surface	gently sloping pahoehoe plates	1.1-1.4
9	Kilauea caldera floor	smooth pahoehoe on caldera floor	
10	Ponded crater floors	smooth ponded flows on pit crater floors	
Lavic Lake Playa		smooth pavement-like surface (4 sites)	0.9-2.1 cm
		average of four sites	1.4 cm

Site numbers keyed to locations in Figure 2. The rms heights for the December 1974 flow are a range over several sample sites from *Gaddis et al.* [1989, 1990]: 2.54 cm horizontal sample intervals, with no high-pass filtering. The rms heights for the 1982 lava flow sites are calculated from data collected at single sites: 5 cm horizontal sample intervals over 5-8 m profile lengths. Range of rms heights shown for 1982 flow data represent standard deviation after a first-order detrending (the high values) and for profiles run through a high-pass filter with a 1 m cutoff wavelength (the low values). Data for Lavic Lake are from four regions of the surface, 10-20 m in extent, measured at horizontal intervals of ~1 cm.

developed layers of glass chips over more competent vesicular rock. On older pahoehoe flows, these chips have eroded away, and only the oxidized interior of the flow remains. A'a flows are comprised of plates or rubble, whose bulk porosity varies with the degree of spiny structure and the weathering of the original clinkers. From the lab studies of *Ulaby et al.* [1988], dielectric values as low as 3-4 might be appropriate for highly vesicular, glassy pahoehoe flows, while values of up to 7 are likely on more competent exposures.

Figures 3-5 show plots of HH versus VV, HV versus LL, and HV versus HH cross section at C, L, and P band wavelengths for all 10 lava flow sites. No effort was made to introduce any kind of incidence angle correction, since to have done so would presuppose a certain scattering regime for the surface. From these plots, we can make several observations.

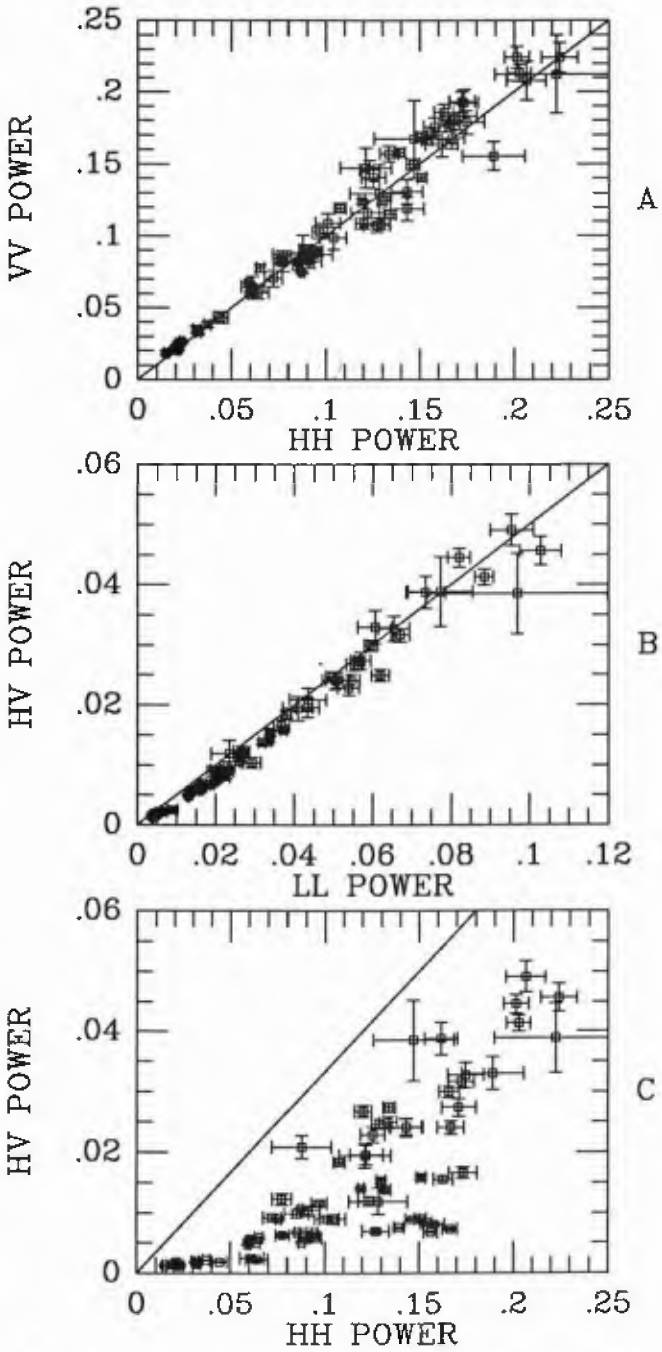

Fig. 3. Plots of (a) HH versus VV, (b) HV versus LL, and (c) HV versus HH backscatter power for C band (5.6 cm) Kilauea data. Linear scaling. Radar incidence angle varies from 27° to 61°, with no corrections made for angular variations in scattering. Error bars represent one standard deviation. Note the close correlation between HH and VV, LL and 2 HV, and the fact that HV echoes never exceed HH/3.

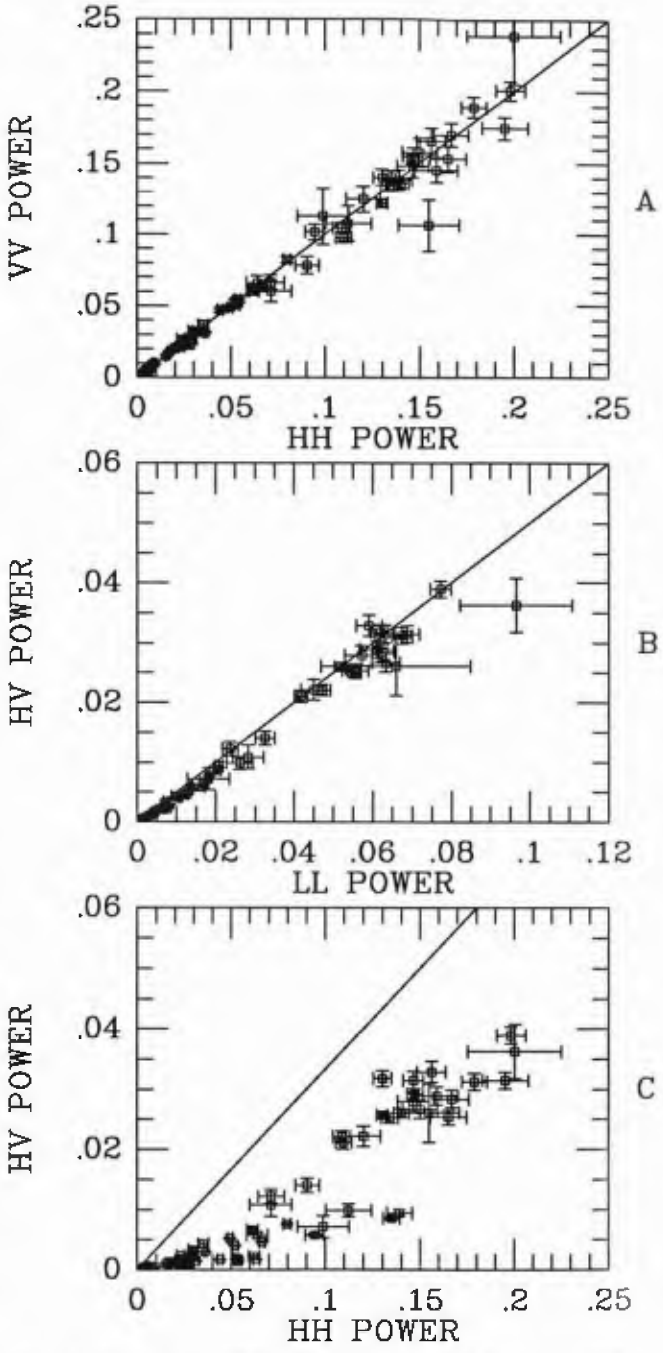

Fig. 4. Plots of (a) HH versus VV, (b) HV versus LL, and (c) HV versus HH backscatter power for L band (24 cm) Kilauea data. Linear scaling. Radar incidence angle varies from 27° to 61°, with no corrections made for angular variations in scattering. Note the close correlation between HH and VV, LL and 2 HV, and the fact that HV echoes never exceed HH/3.

1. At C and L band, the HH and VV cross sections are very well correlated, and follow a 1:1 trend. An examination of the HH/VV ratio images showed that there is no geologic significance to deviations from the 1:1 trend over the lava flows (vegetated and ash-covered regions do exhibit a range of HH/VV behaviors). At P band, the VV echoes are often greater than the HH returns (they fall above the 1:1 line in Figure 3*c*),

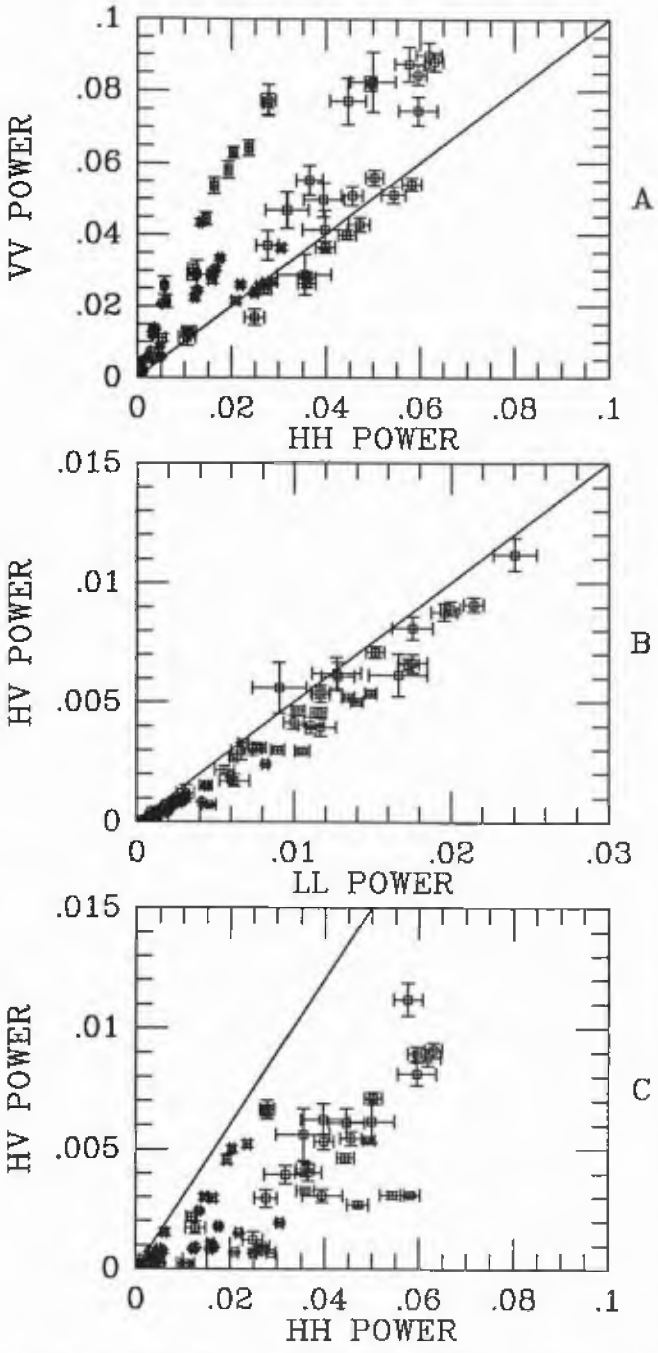

Fig. 5. Plots of (a) HH versus VV, (b) HV versus LL, and (c) HV versus HH backscatter power for *P* band (68 cm) Kilauea data. Linear scaling. Radar incidence angle varies from 27° to 61°, with no corrections made for angular variations in scattering. Note the enhancement of VV over HH, in contrast to the *C* and *L* band data shown in Figures 3 and 4.

but variations in the HH/VV ratio are again not well correlated with lava flow unit boundaries.

2. At all three radar wavelengths, the LL and HV echoes fall close to a 2:1 line (LL=2 HV). The fit to this line is very good at *C* and *L* band, while at *P* band the LL echoes are typically slightly greater than twice the HV returns.

3. For all three wavelengths and over all study sites the HH echoes are greater than 3 HV. There is a trend toward higher HV/HH ratios on rougher surfaces and at shorter wavelengths.

The lava flow polarization properties observed for *C* and *L* band wavelengths (HH = VV, LL = 2 HV, and HH>3 HV) are consistent with scattering by a combination of the quasi-specular (or small facet) and diffuse mechanisms. The small-perturbation and dihedral/coherent models seem unlikely to play a major role, since they contribute unequally to HH and VV, and would tend to enhance LL significantly over the dipole mechanism's prediction of 2 HV. The small facet mechanism is proposed as the source of the nondiffuse HH and VV echoes, since at the 30-60° incidence angles of these measurements few large radar-facing facets are expected. The two scattering components may be separated by calculating the small facet contribution:

$$\sigma_0^f = \mathrm{HH} - 3\,\mathrm{HV} \tag{19}$$

and the fraction of the echo which is due to small facet returns may be found by dividing this cross section by the HH return.

Figures 6 and 7 show the facet component cross section (19) and the fraction of facet scattering for *C* and *L* band images of Kilauea. The facet cross section is generally greater at *C* band than at *L* band. The fraction of facet return is greater at *L* band for most surfaces, but the *C* and *L* band fractions are similar (nearly zero) for the roughest a'a flows. The lower average facet fraction at *C* band is probably due to a rise in diffuse scattering with shorter radar wavelengths which exceeds the increase in facet returns at these smaller scales. Tests with data from other flightlines showed that the facet component rises sharply with decreasing incidence angle, as expected from the discussion above.

It is interesting to note that many of the flow units cannot be distinguished on the basis of their facet-scattered echo. This could be explained by considering the distribution of roughness on such surfaces. While the pahoehoe flows are typically much smoother at scales of a few centimeters (and should thus offer a strong specular return), they rarely have sufficient long-wavelength roughness to offer many facets at high incidence angles. In contrast, the rougher flows have infrequent smooth reflecting areas, but a much greater number of surfaces tilted at high angles. The total number of small facets thus appears to be nearly equal over a wide range of roughnesses. This effect is most pronounced at *C* band, with a slight improvement in unit discrimination at *L* band.

At *P* band, many of the flow surfaces have VV backscatter cross sections which are greater than their HH returns, and LL echoes slightly greater than 2 HV. Based on the discussion of scattering mechanisms above, this might be explained by (1) some component of small-perturbation scattering, or (2) penetration of the radar energy into the surface and scattering within the lava. We can test both possibilities using the scattering model polarization properties and applicabilities discussed above.

In order to satisfy the requirements of the first-order small-perturbation model for a 68-cm radar wavelength, the surface would need to have an rms height less than 3.5 cm. This criterion is exceeded by even the moderately rough pahoehoe flows (Table 1), so the model is strictly applicable only to the smoothest lava surfaces. It is clear from Figure 5a, however, that the enhancement of VV over HH occurs most strongly at intermediate backscatter powers. These two observations suggest that the small-perturbation model is not appropriate to explain the scattering from the lava flows at *P* band. As a final test, we can assume that the backscatter can be written as the sum of facet, small-perturbation, and diffuse components:

$$\mathrm{HH} = \mathrm{F} + \mathrm{D_{hh}} + \mathrm{S} \tag{20}$$

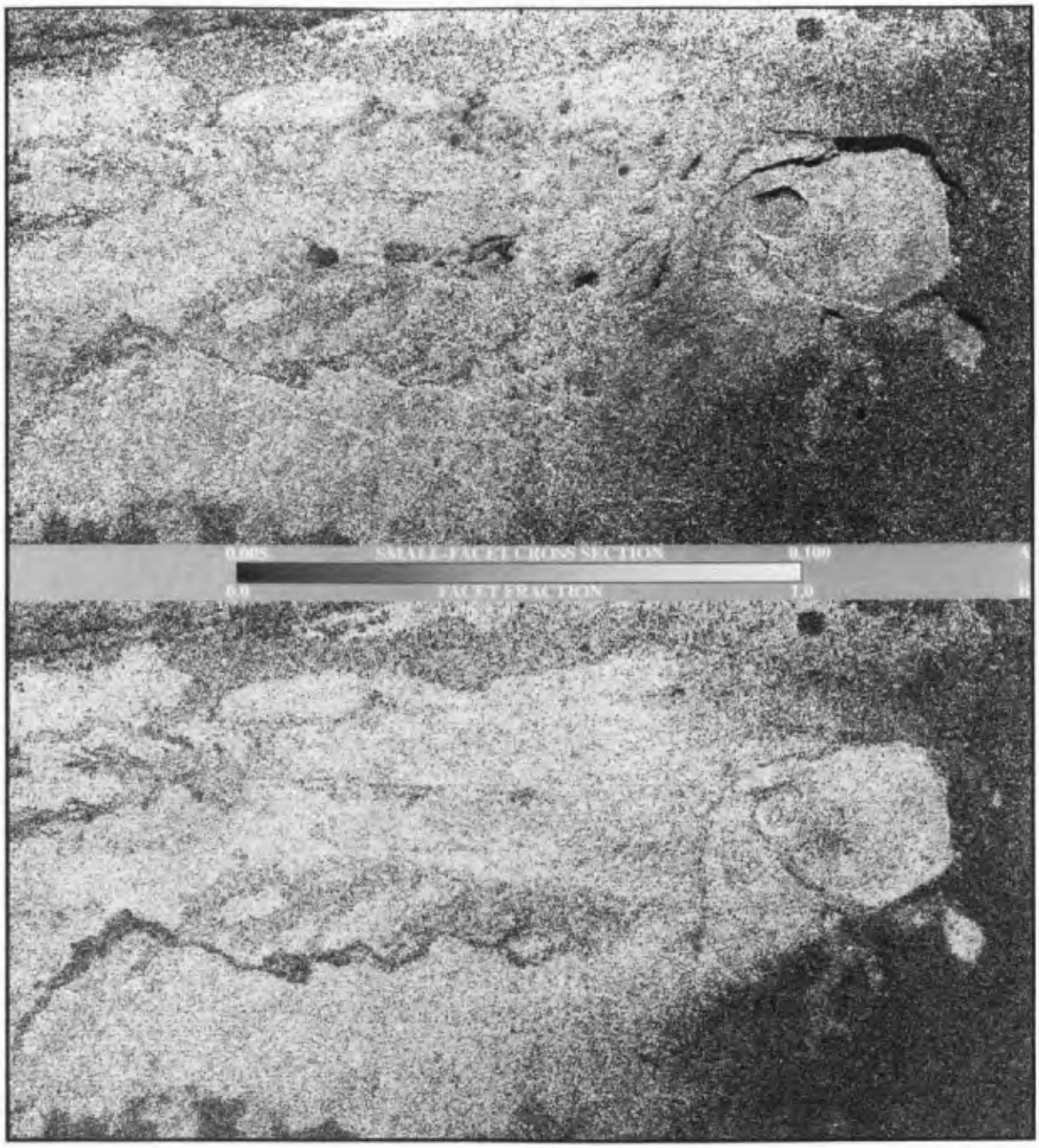

Fig. 6. Images of (a) facet scattering cross section (HH-3 HV) and (b) facet scatter fraction (HH-3 HV)/HH for Kilauea summit and Kau desert. Radar wavelength 5.6 cm (*C* band); incidence angle range approximately 38° to 48° in this scene. Cross section presented with stretch (black, 0.005; white, 0.1), logarithmic scaling. Ratio image stretched (black, 0.0; white, 1.0), linear scaling.

$$VV = F + D_{vv} + S\left(\frac{\alpha_{vv}^2}{\alpha_{hh}^2}\right) \tag{21}$$

$$LL = D_{ll} + S\left(\frac{\alpha_{ll}^2}{\alpha_{hh}^2}\right) \tag{22}$$

where F is the facet component (equal in HH and VV), S is the amount of HH return due to the small-perturbation model, and D_{ij} is the diffuse return at the given polarization (see equations 7-10 for definitions of the α terms). The diffuse components are assumed to be: $D_{hh}=D_{vv}=3$ HV, $D_{ll}=2$ HV. If this model is accurate, then the HH, VV, and LL terms may be used to derive values for F, S, and the surface dielectric constant. We have neglected the coherent scattering effect in this analysis because it seems unlikely that multiple scattering from the jagged lava flow surface will produce strong echoes. The VV return must be higher than the HH return for this model to have positive solutions for all three components. If this condition is satisfied, the dielectric constant ε can be obtained from

$$\frac{(VV - HH)}{(LL - 2HV)} = 4\frac{\alpha_{vv}^2 - \alpha_{hh}^2}{\left[\alpha_{hh} - \alpha_{vv}\right]^2} \tag{23}$$

since the right-hand side depends only on ε and the incidence angle. For the P band Kilauea lava flow data, the values presented in Figure 5 require dielectric constants >20, which are not reasonable for dry basalt rocks [*Ulaby et al.*, 1988].

The second possible mechanism for the enhanced P band VV echoes is radar penetration and volume scattering. If we

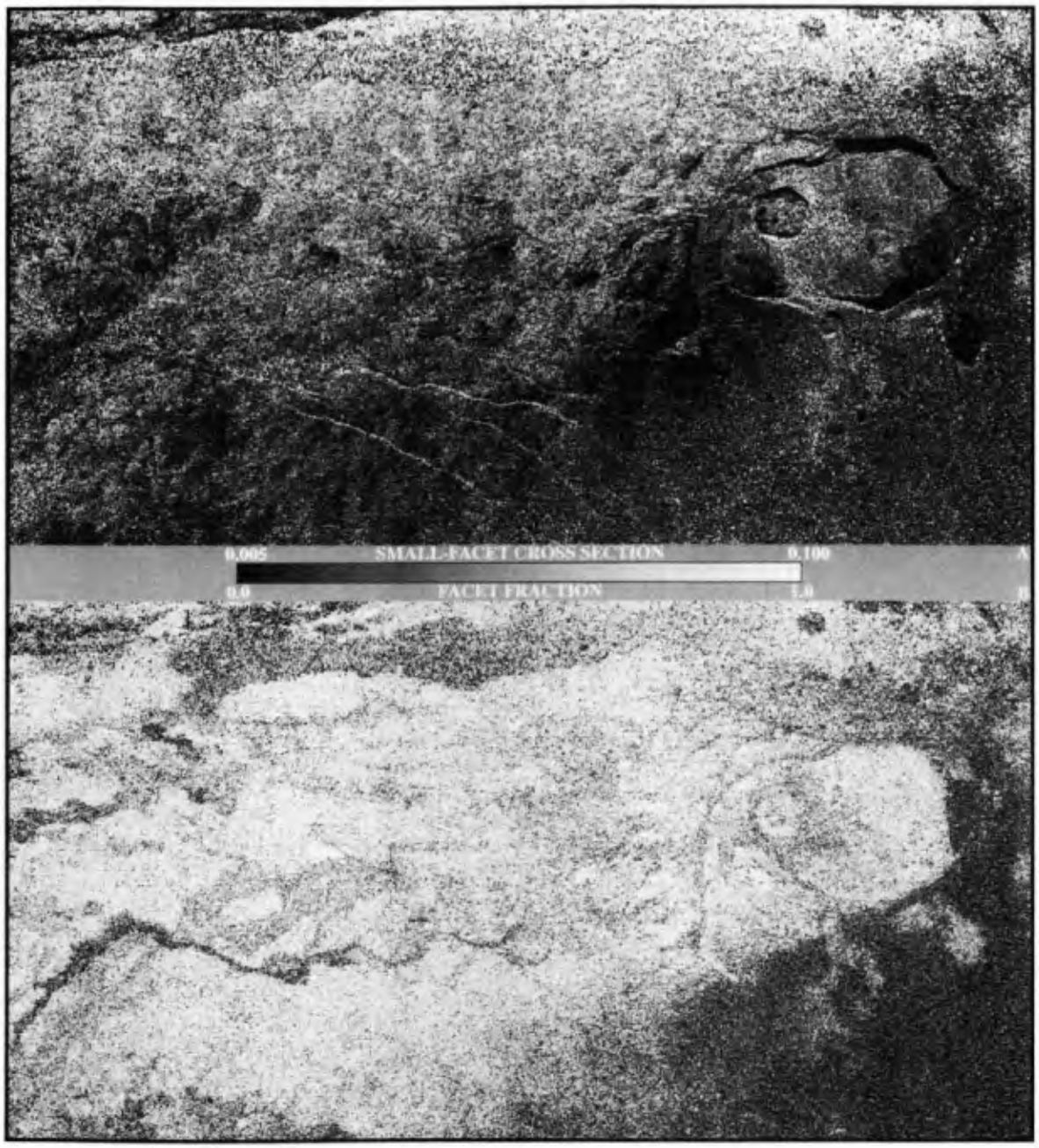

Fig. 7. Images of (a) facet scattering cross section (HH-3 HV) and (b) facet scatter fraction (HH-3 HV)/HH for Kilauea summit and Kau desert. Radar wavelength 24 cm (*L* band). Cross section presented with stretch (black, 0.005; white, 0.1), logarithmic scaling. Ratio image stretched (black, 0.0; white, 1.0), linear scaling.

assume that any scattering within the lava flow is similar to a random-dipole case, then the polarization properties of this component of the backscattered wave are given by (16)-(18). The passage of the radar through the surface twice on its path back to the receiver will tend to favor VV polarization, since HH is preferentially forward-scattered at any dielectric interface. Such penetration could easily produce the observed VV/HH ratios of up to 2:1 seen for the Kilauea flows with lava dielectric constants of 7 or less. If the volume scattering is similar to the random dipole case, then we would expect no change in the HV or LL cross sections due to the interface, consistent with the 2:1 behavior seen in Figure 5*b*. This scattering model thus seems to better fit the observations than the first-order small-perturbation mechanism. It is not expected that radar penetration should enhance VV efficiently on very rough terrain, where the local mean surface has a wide range of orientations to the incident wave. The tendency for the HH and VV returns to become more similar at higher brightnesses (Figure 5*a*) is consistent with this model.

SP Flow

SP flow in northern Arizona is a blocky basaltic andesite lava deposit [*Schaber et al.*, 1980]. The surface is characterized by roughly cubical blocks, 0.1-1.0 m in size, whose sides are smooth on the scale of a few centimeters. The lava is massive, with few vesicles or pore spaces, and there is no broken glass

coating as is seen on many of the Hawaiian lava flows. The dielectric constant for this flow is thus taken to be 6-8 [*Ulaby et al.*, 1988]. Figure 8 presents an *L* band HH AIRSAR image of this flow. We did not use the *C* band data for this site, as there were questions about the validity of the antenna beam pattern correction.

If we average over large regions of the blocky terrain, we find the following.

1. The *L* band echoes for SP flow are similar in behavior to those of the Kilauea lavas (Figure 9), and again we propose a combination of diffuse and small-facet scattering mechanisms. The inferred facet scattering component is relatively slight, as shown by the small enhancements of HH over 3 HV (Figure 9c).

2. The *P* band data for SP flow (Figure 10) show the same enhancement of VV over HH seen for the Kilauea surfaces, and again have LL/HV ratios close to 2. The greatest VV enhancements occur at the lower radar brightnesses, with the roughest areas having HH/VV ratios close to unity. As we discussed above, the radar penetration/volume scattering model seems to better fit the observation of enhanced VV echoes at 68-cm wavelength. Again, the issue of a highly variable local mean surface arises, but we do see the roughest terrains moving toward uniform HH and VV returns.

On the local level, SP flow exhibits wide variations in LL/LR ratio about unity at 24-cm wavelength. Even when the data are averaged in 5x5 pixel bins to limit speckle effects, there are significant areas of the flow with LL/LR ratios greater than unity (Figure 11). There is no correlation between the LL/LR and HH/VV ratios across the flow surface; HH/VV values appear to be randomly distributed between ~0.6 and 1.6. HV/LL ratios remain very close to 0.5 throughout the flow. The anomalously high LL/LR ratio values may be attributable to dihedral double-bounce returns or to the coherent backscattering phenomenon. The latter model seems more likely since it requires no favorable orientation for the scattering elements and does not imply consistently high HH/VV ratios, which are not observed (Figure 9*a*).

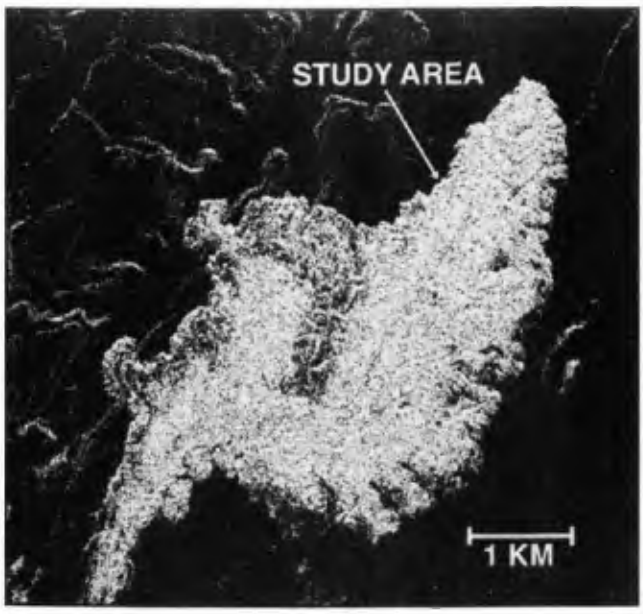

Fig. 8. *L* band (24 cm) HH radar image of SP flow in northern Arizona. Image width 6 km, with radar flightline across top. Image center approximately 111° 25' W, 35° 48' N. Sample data taken from large bright flow lobe, shown by arrow. Logarithmic scaling, slant-range projection.

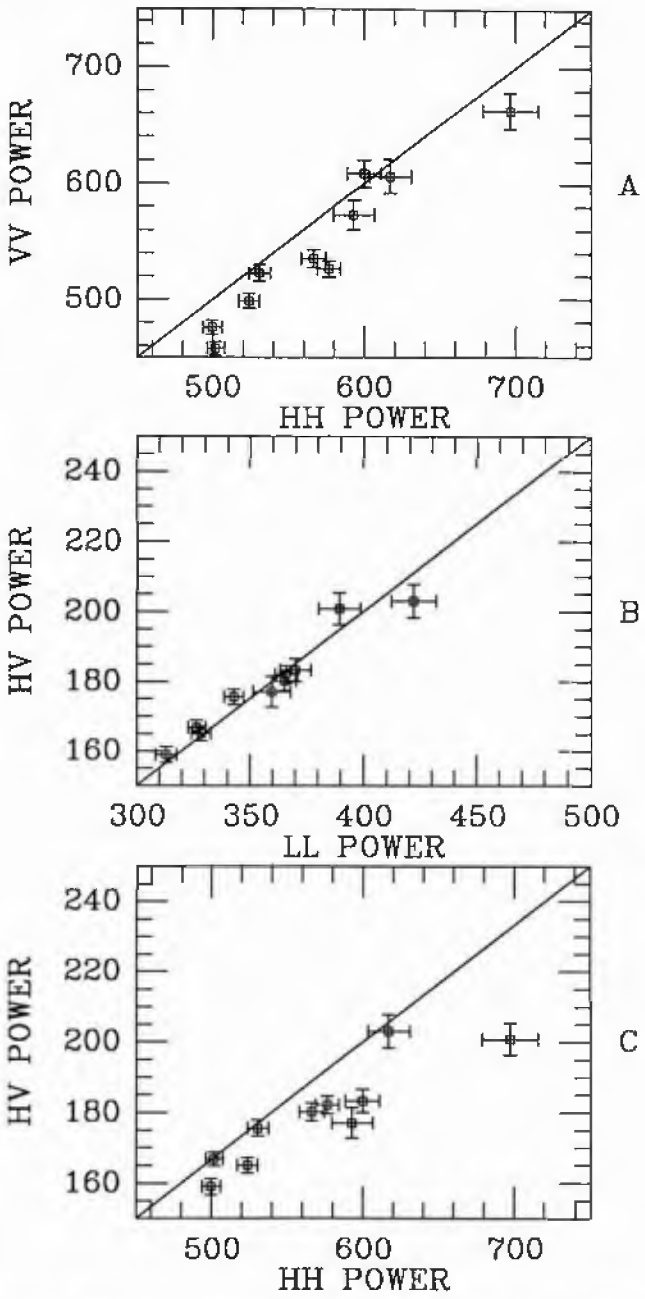

Fig. 9. Plots of (a) HH versus VV, (b) HV versus LL, and (c) HV versus HH backscatter power for *L* band SP flow data. Backscatter cross sections in arbitrary units, with linear scaling. Incidence angle range 42°-53°.

Summary

We can model the radar echoes from all of the lava flows at *C* and *L* band as the sum of facet and dipole components. We propose that scattering by small facets is an important mechanism at oblique (>20°) incidence angles. The first-order small-perturbation model does not match the backscatter from the flows because their surface roughness exceeds the validity conditions of the model at *C* and *L* band. Enhancement of the VV backscatter cross section for some flows at *P* band is tentatively attributed to radar penetration and volume

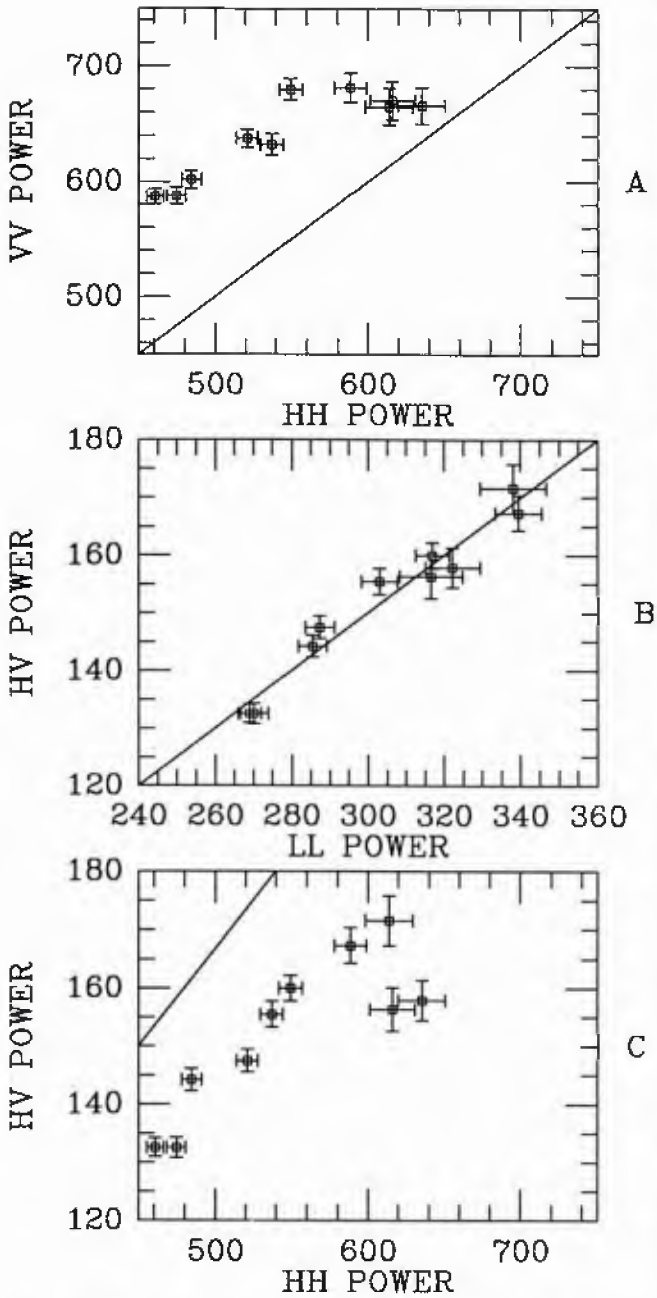

Fig. 10. Plots of (a) HH versus VV, (b) HV versus LL, and (c) HV versus HH backscatter power for *P* band SP flow data. Backscatter cross sections in arbitrary units, with linear scaling. Incidence angle range 42°-53°.

scattering. SP flow shows localized evidence for possible coherent backscattering.

Radar Observations Of Playa Surfaces

Lavic Lake Playa

The first lacustrine surface we examined is the Lavic Lake playa in the Pisgah volcanic field, California. This surface is characterized by rms surface heights of ~1.4 cm, primarily in the form of polygonal mud cracks (Table 1, Figure 12) [*Arvidson et al.*, 1993]. Field probe measurements indicate a real dielectric constant of 2.36 for this surface [*van Zyl et al.*, 1991], but the actual values are likely quite variable due to changes in moisture content.

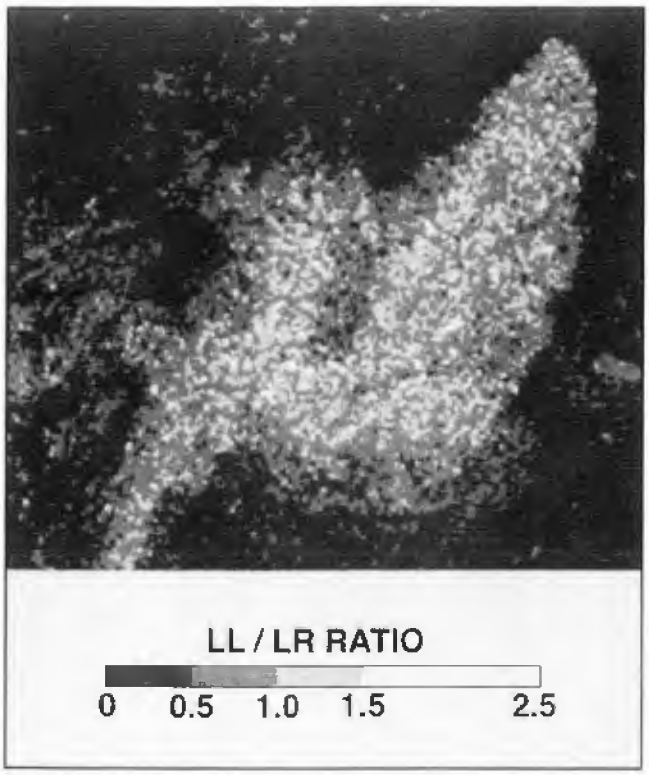

Fig. 11. *L* band (24 cm) LL/LR ratio image for SP flow after 5x5 boxcar filtering of raw 4-look data. Image stretched to highlight regions where LL/LR ratios exceed unity.

Radar backscatter values for the study region, outlined in Figure 12, were binned every 1° of incidence angle. Figure 13 shows the polarization ratios calculated from the image data, and for cross sections modified to take into account a maximum possible diffuse scattering component. In each case, these values represent the ratio of mean LL echo to mean LR

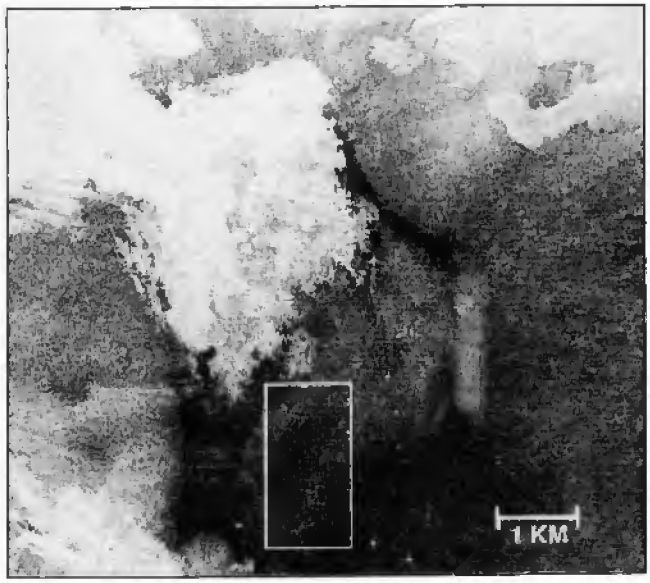

Fig. 12. *L* band radar image of Lavic Lake playa region, with the location of the sample area outlined in white. Slant-range projection, logarithmic image scaling. Image width 8 km, with flightline across top. Image center approximately 116° 26' W, 34° 45' N. The very bright points on the playa surface are corner reflectors.

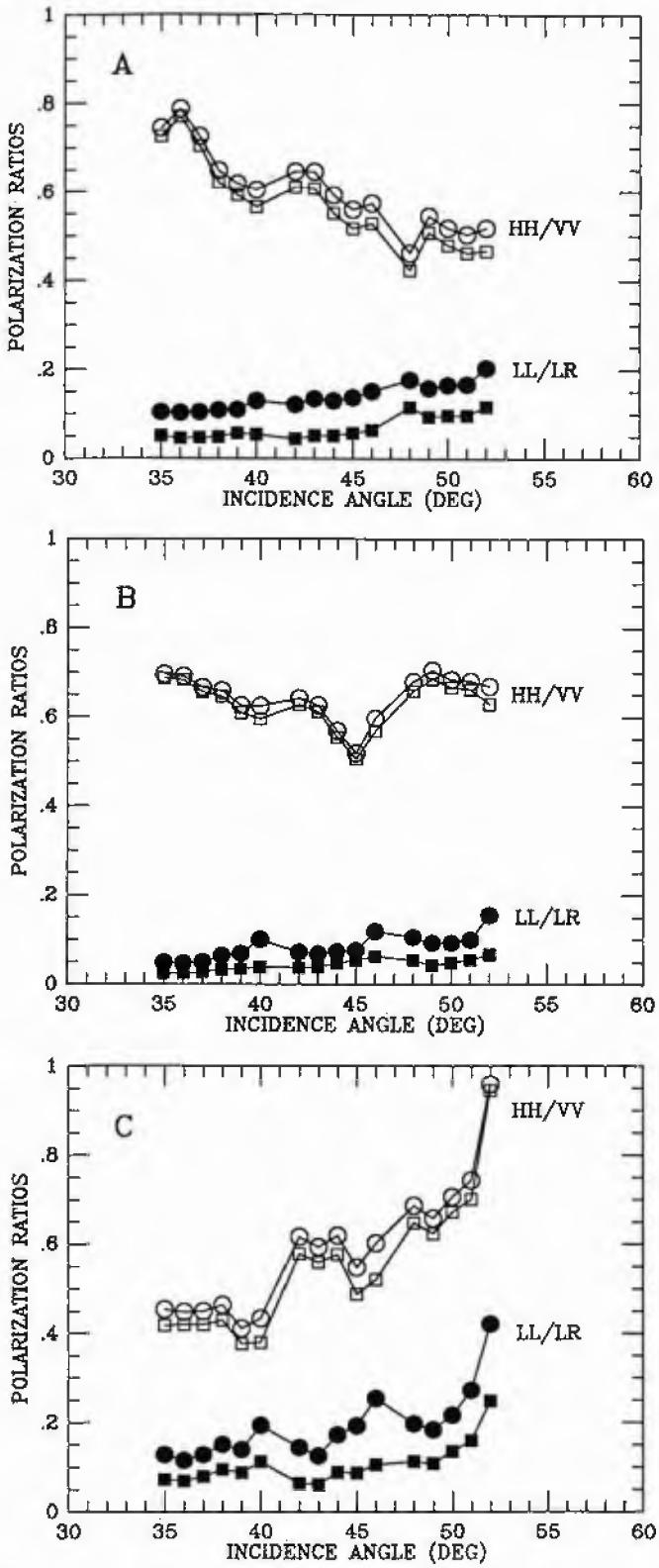

Fig. 13. Plots of HH/VV, (HH-3 HV)/(VV-3 HV), LL/LR, and (LL-2 HV)/(LR-2 HV) ratios versus incidence angle for Lavic Lake sites. (a) C band, (b) L band , (c) P band. Note the relatively poor correlation between these plots and the model-derived values shown in Figure 1.

echo (not the mean ratio). Comparing these data to Figures 1 and 2, we find the following.

1. the HH/VV ratios at *C* band (all angles) and *L* band (out to ~45°) are close to the values predicted by the first-order small-perturbation model for a dielectric constant of 2. A similar dielectric constant is inferred after subtraction of the possible diffuse component (3 HV). The LL/LR ratio values at *C* and *L* band correspond to dielectric constants of 5-7. After removal of the diffuse component (2 HV), the *C*-band LL/LR ratios match the small-perturbation model for dielectric constants of 3-7, depending upon the incidence angle. At *L* band, the corrected LL/LR ratios fit a dielectric constant value of ~3.

2. At *P* band, the HH/VV ratio increases with incidence angle, which would not be expected for small-perturbation scattering. The LL/LR ratio values, even after correction for diffuse scattering, would require dielectric constants greater than 7.

These results suggest that a simple two-component (diffuse and first-order small-perturbation) model cannot explain the scatter from the playa surfaces. While the results at *L* band do approximate the model predictions for a dielectric constant of 2-3, the goodness of fit varies with incidence angle. The *P* band measurements are completely inconsistent with the small-perturbation model. It seems likely that there is some degree of radar volume scattering within the playa surface, particularly at *L* and *P* band wavelengths. The first-order small-perturbation model cannot be used by itself to infer roughness properties, but a thorough inverse model might require more parameters than we have degrees of freedom in the data.

The Pisgah playa and lava flows were used to test an inversion technique, based on the first-order small-perturbation model, by *van Zyl et al.* [1991], who found some correlation between measured surface power spectral density (PSD) and the radar-derived topographic components. This result is inconsistent with the rms heights of the study surfaces, the analysis of *Gaddis* [1992], and our results, all of which suggest that the small-perturbation model is not applicable to the Pisgah terrains. The fit between modeled and measured PSD's for the lava flows may thus be fortuitous.

Lunar Lake Playa

The second playa surface we studied is in the Lunar Crater Volcanic field, Nevada. Data for this area were collected as part of the Geoscience Remote Sensing Field Experiment (GRSFE) experiment [*Dale-Bannister and Arvidson*, 1991]. This surface is also extremely smooth, with roughness heights (inferred from stereo photography profiles) typically less than 1 cm. Figure 14 shows a *C* band HH AIRSAR scene of the playa, with the sample region outlined. Figure 15 presents the polarization ratios for this surface, before and after removal of the maximum possible diffuse component. At *P* band it appeared that the backscatter cross sections were at the level of the system noise for incidence angles >45°, since the ratios beyond this point fluctuated wildly. We have thus cut off the data plotted in Figure 15c at 45°.

The scattering properties of this playa are generally similar to those of the Lavic Lake area, but the fit to the first-order small-perturbation model is even worse.

1. The LL/LR ratios for Lunar Lake at all three wavelengths can only fit the small perturbation model with dielectric constants of 7 or more, even after removal of an assumed diffuse contribution.

2. HH/VV ratios imply dielectric constant values of 2-6. Only at *L* band do the HH/VV ratios follow the model-predicted trend (Figure 1) well. For the *P* band data, the HH/VV ratios rise with increasing incidence angle.

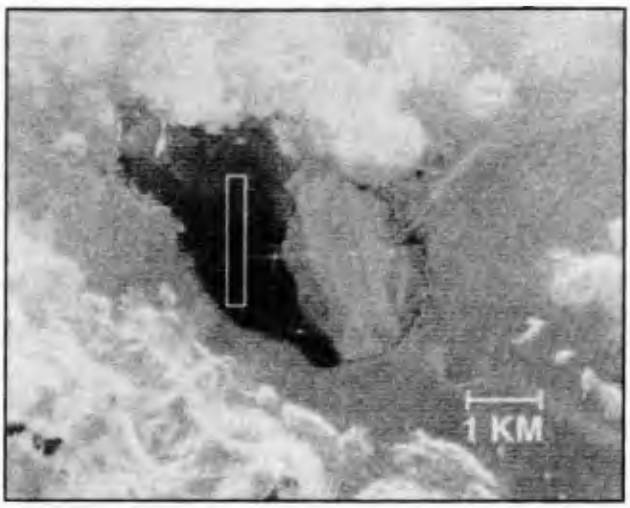

Fig. 14. *L* band radar image of Lunar Lake playa region, with the location of the sample region outlined in white. Slant-range projection, logarithmic image scaling. Image width 8 km, with flightline across top. Image center approximately 116° 1' W, 38° 22' N. The very bright points on the playa are corner reflectors.

Summary

The playa surfaces are characterized by polarization ratios which are, at best, qualitatively consistent with some predictions of the first-order small-perturbation scattering model. The polarization properties do not, however, fit this model to the degree necessary for reliable inverse modeling. Even compensating for the assumed diffuse echo does not bring the data in line with the model predictions. Radar volume scattering within the playa surfaces or higher-order expansions of the perturbation model could provide a means for explaining the observed returns, but these mechanisms are not easily cast in an invertible model.

DISCUSSION

Implications for Venus Data Interpretation

Magellan collected VV polarization data during portions of its second and third mission cycles. Some of these data have been analyzed by *Plaut* [1993], who found significant enhancements of VV over HH in some areas of high Fresnel reflectivity. This type of behavior may be consistent with small-perturbation scattering from very smooth surfaces with high dielectric constants, but further work is needed to assess the occurrence of these polarization anomalies and their correlation with Arecibo circular-polarized images. The combination of the two data sets should provide sufficient information to test the utility of various scattering models to these high-reflectivity surfaces. The Arecibo circularly-polarized data should also be a useful gauge of the facet and diffuse scattering components on most lava flows [*Campbell and Campbell*, 1992] because both returns are linked to single-scattering mechanisms. In regions of high reflectivity, this may not be the case. The high circular polarizations ratios (>1.0) seen for the Maxwell Montes may be due to coherent multiple scattering from surface rocks with high Fresnel reflectivities. The returns from SP flow approach the types of depolarized circular enhancements seen for the Venus highlands, and the elevated dielectric constants in these regions should favor the multiple-scattering mechanism.

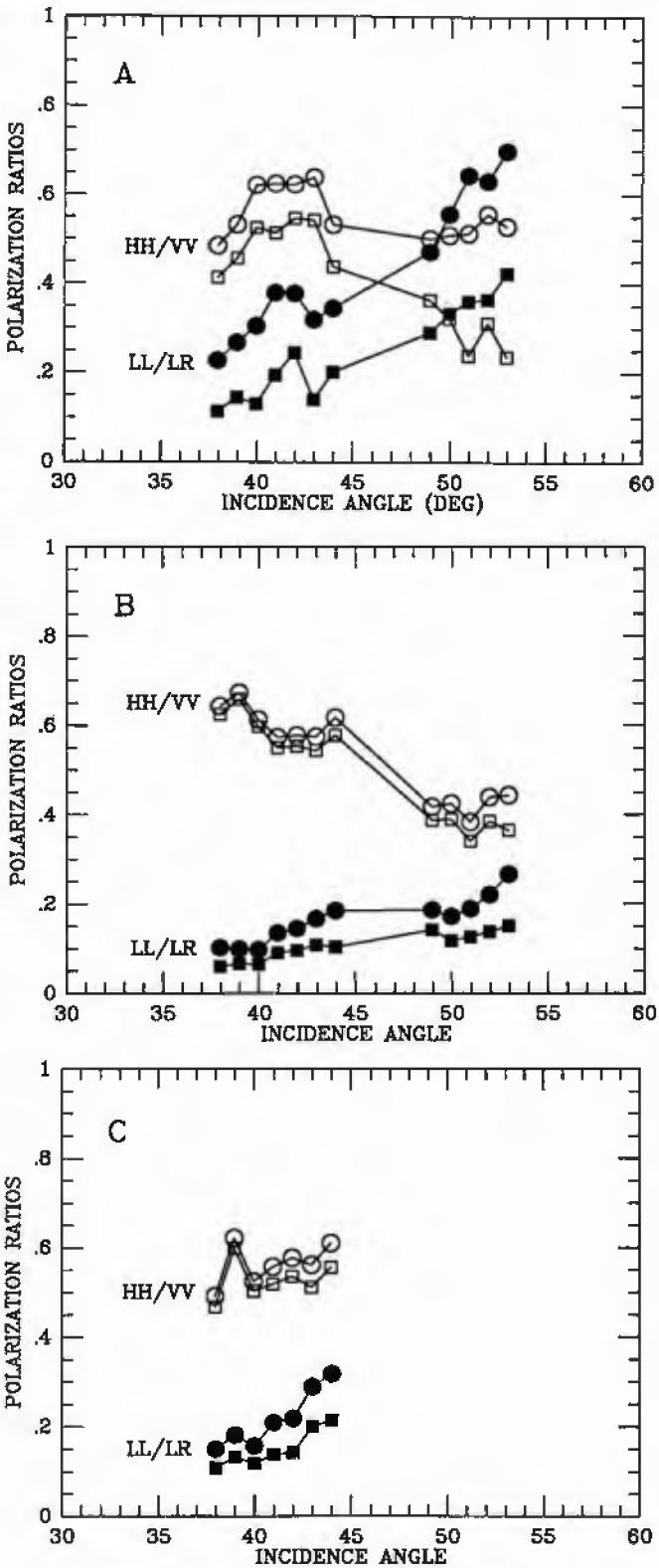

Fig. 15. Plots of HH/VV, LL/LR, (HH-3 HV)/(VV-3 HV), and (LL-2 HV)/(LR-2 HV) ratio values versus incidence angle for Lunar Lake. *P* band data truncated at 45° incidence angle, as values beyond this seemed to be in the noise. Note the relatively poor correlation between these plots and the model-derived values shown in Figure 1.

The fact that part of the HH return at oblique incidence angles may not be diffuse must be considered when analyzing the "tail" of a backscatter distribution (ϕ>20°), where one would expect the quasi-specular echoes to be very low. Our

results suggest that the magnitude and shape of the backscatter function at oblique incidence angles is a combination of diffuse (dipole-like) echoes and small-facet returns. In current algorithms for PVO and Magellan altimeter-derived reflectivity corrections, the observed nadir return is scaled by the amount of energy inferred to have been scattered by rough terrain [*Pettengill et al.*, 1988]. Further work is needed to assess the degree to which the "small-facet" return may bias estimates of this rough-surface fraction.

Implications for Terrestrial Remote Sensing

For terrestrial geologic remote sensing, these results show that developing an inverse model for the polarization properties of a surface may be relatively simple, as was seen for the Kilauea lava flows at C and L band where only two components are needed. In the playa regions, no simple invertible model was found, presumably due to significant volume scattering or roughness which did not satisfy the first-order small-perturbation criteria. The use of the small-perturbation model for direct inference of the roughness and dielectric parameters of a lava surface [*van Zyl et al.*, 1991] is not supported by these data. The four-component invertible model proposed by *Campbell et al.* [1989] treats the diffuse (dipole) echo component as a single polarization-independent power; from the results shown here, it should be different for linear and circular polarization states. Volcanic surfaces with roughness greater than ~1 cm can be modeled at *C* and *L* band by a simple combination of diffuse and facet scattering, requiring only HH and HV (or VV and VH) data for the analysis. Fully polarimetric data are needed to discriminate bare lava from weathered soil, ash, or other porous material.

Acknowledgments. The authors thank Jim Garvin for much assistance in collecting the Kilauea field topography data. Thanks also to Tom Farr for calibrating the Hawaii AIRSAR data, and to Don Campbell and Nick Stacy for helpful discussions. Lisa Gaddis and Peter Ford provided very thorough and helpful reviews. R.E.A. and M.K.S. were supported by NASA Planetary Geology and Geophysics Program grant NAGW-1087 for Washington University. Portions of this work were also supported by NASA Planetary Geology and Geophysics Program grant NAGW-3360.

REFERENCES

Arvidson, R.E., R. Greeley, M. Malin, R.S. Saunders, N. Izenberg, J.J. Plaut, E.R. Stofan, and M.K. Shepard, Surface modification of Venus as inferred from Magellan observations of plains, *J. Geophys. Res.*, *97*, 13303-13318, 1992.

Arvidson, R., M. Shepard, E. Guiness, S. Petroy, J. Plaut, D. Evans, T. Farr, R. Greeley, N. Lancaster, and L. Gaddis, Characterization of lava flow degradation in the Pisgah and Cima volcanic fields, California, using Landsat Thematic Mapper and AIRSAR data, *Geol. Soc. Am. Bull.*, *105*, 175-188, 1993.

Barrick, D.E., and W.H. Peake, Scattering from surfaces with different roughness scales: Analysis and interpretation, *Rep. 1388-26*, Ohio State Univ. Electrosci. Lab., Columbus, 1967.

Blom, R.G., L.R. Schenck, and R.E. Alley, What are the best radar wavelengths, incidence angles, and polarizations for discrimination among lava flows and sedimentary rocks? A statistical approach, *IEEE Trans. Geosci. RemoteSens., GE-25*, 2208-2213, 1987.

Campbell, B.A., and D.B. Campbell, Analysis of volcanic surface morphology on Venus from comparison of Arecibo, Magellan, and terrestrial airborne radar data, *J. Geophys. Res.*, *97*, 16,293-16,314, 1992.

Campbell, B.A., and J.B. Garvin, Lava flow topographic measurements for radar data analysis, *Geophys. Res. Lett.*, *20*, 831-834, 1993.

Campbell, B.A., S.H. Zisk, and P.J. Mouginis-Mark, A quad-pol radar scattering model for use in remote sensing of lava flow morphology, *Remote Sens. Environ.*, *30*, 227-237, 1989.

Campbell, D.B., N.J.S. Stacy, W.I. Newman, R.E. Arvidson, E.M. Jones, G.S. Musser, A.Y. Roper, and C. Schaller, Magellan observations of extended impact crater related features on the surface of Venus, *J. Geophys. Res.*, *97*, 16,249-16,278, 1992.

Dale-Bannister, M.A., and R.E. Arvidson, Magellan data released on PDS node, *Eos Trans. AGU*, *72*, 490-491, 1991.

Evans, D.L., *et al.*, The Shuttle Imaging Radar-C and X-SAR mission, *Eos Trans. AGU*, *74*, 145-158, 1993.

Evans, D.L., T.G. Farr, J.P. Ford, T.W. Thompson, and C.L. Werner, Multipolarization radar images for geologic mapping and vegetation discrimination, *IEEE Geosci. Remote Sens., GE-24*, 246-257, 1986.

Ford, P.G., and G.H. Pettengill, Venus topography and kilometer-scale slopes, *J. Geophys. Res.*, *97*, 13,102-13,114, 1992.

Ford, P.G., and D.A. Senske, The radar scattering characteristics of Venus landforms, *Geophys. Res. Lett.*, *17*, 1361-1364, 1990.

Freeman, A., J.J. van Zyl, J.D. Klein, H.A. Zebker, and Y. Shen, Calibration of Stokes and scattering matrix format polarimetric SAR data, *IEEE Geosci. Remote Sens.*, *30*, 531-539, 1992.

Fung, A.K., Z. Li, and K.S. Chen, Backscattering from a randomly rough dielectric surface, *IEEE Geosci. Remote Sens.*, *30*, 356-369, 1992.

Gaddis, L.R., Lava flow characterization at Pisgah volcanic field, California, with multiparameter imaging radar, *Geol. Soc. Am. Bull.*, *104*, 695-703, 1992.

Gaddis, L.R., P.J. Mouginis-Mark, R. Singer, and V. Kaupp, Geologic analyses of SIR-B data of Kilauea Volcano, Hawaii, *Geol. Soc. Am. Bull.*, *101*, 317-332, 1989.

Gaddis, L.R., P.J. Mouginis-Mark, and J.N. Hayashi, Lava flow surface textures: SIR-B radar image texture, field observations, and terrain measurements, *Photogramm. Eng. Remote Sens.*, *56*, 211-224, 1990.

Hagfors, T., Backscattering from an undulating surface with applications to radar returns from the Moon, *J. Geophys. Res.*, *69*, 3779-3784, 1964.

Hagfors, T., A study of the depolarization of lunar radar echoes, *Radio Sci.*, *2*, 445-465, 1967.

Hagfors, T., and J.V. Evans, Radar studies of the Moon, in *Radar Astronomy*, pp. 219-273, McGraw-Hill, New York, 1968.

Hapke, B., Coherent backscatter and the radar characteristics of outer planet satellites, *Icarus*, *88*, 407-417, 1990.

Head, J.W., L.S. Crumpler, J.C. Aubele, J.E. Guest, and R.S. Saunders, Venus volcanism: Classification of volcanic features and structures, associations, and global distribution from Magellan data, J. Geophys. Res., 97, 13,153-13,197, 1992.

Mack, C.L., and B. Reiffen, RF characteristics of thin dipoles, *Proc. IEEE*, *52*, 533-542, 1964.

Ostro, S.J., *et al.*, Europa, Ganymede, and Callisto: New radar results from Arecibo and Goldstone, *J. Geophys. Res.*, *97*, 18,227-18,244, 1992.

Pettengill, G.H., P.G. Ford, and B.D. Chapman, Venus: Surface electromagnetic properties, *J. Geophys. Res.*, *93*, 14,881-14,892, 1988.

Pettengill, G.H., P.G. Ford, and R.J. Wilt, Venus surface radiothermal emission as observed by Magellan, *J. Geophys. Res.*, *97*, 13,091-13,102, 1992.

Plaut, J.J., Radar scattering as a source of geological information on Venus and Earth, PhD. Dissertation, Washington Univ., St. Louis, MO., 1991.

Plaut, J.J., Magellan vertical polarization radar observations, *Lunar Planet Sci. Conf. XXIV*, 1151-1152, 1993.

Saunders, R.S., *et al.*, Magellan mission summary, *J. Geophys. Res.*, *97*, 13067-13090, 1992.

Schaber, G.G., C. Elachi, and T.G. Farr, Remote sensing of SP mountain and SP lava flow in North-central Arizona, *Remote Sens. Environ.*, *9*, 149-170, 1980.

Stratton, J.A., *Electromagnetic Theory*, John Wiley, New York, 1947.

Theilig, E., S. Wall., and R.S. Saunders, Radar interpretation of lava fields as a function of incidence angle: Implications for intepretation of Magellan SAR data of Venus, *Lunar Planet. Sci. Conf., XIX*, 323-335, 1989.

Tyler, G.L., R.A. Simpson, M.J. Maurer, and E. Holmann, Scattering properties of the Venus surface: Preliminary results from Magellan, *J. Geophys. Res.*, *97*, 13115-13140, 1992.

Ulaby, F.T., R.K. Moore, and A.K. Fung, *Microwave Remote Sensing*, Addison-Wesley, Reading, Mass., 1987.

Ulaby, F.T., T. Bengal, J. East, M.C. Dobson, J. Garvin, and D. Evans, Microwave dielectric spectrum of rocks, *Rep. 23817-1-T*, 81 pp., Univ. of Mich. Radiation Lab., Ann Arbor, 1988.

van Zyl, J.J., Unsupervised classification of scattering behavior using radar polarimetry data, *IEEE Geosci. Remote Sens., 27*, 36-45, 1989.

van Zyl, J.J., Calibration of polarimetric radar images using only image parameters and trihedral corner reflector responses, *IEEE Trans. Geosci. Remote Sens., 28*, 337-348, 1990.

van Zyl, J.J., C.F. Burnette, and T.G. Farr, Inference of surface power spectra from inversion of multifrequency polarimetric radar data, *Geophys. Res. Lett., 18*, 1787-1790, 1991.

R.E. Arvidson and M.K. Shepard, Department of Earth and Planetary Sciences, Washington University, St. Louis, MO 63130.

B.A. Campbell, Center for Earth and Planetary Studies, National Air and Space Museum, Washington, DC 20560.

(Received October 1, 1992;
revised April 20, 1993;
accepted June 8, 1993.)